nature cell biology

Coupling between clathrin-dependent endocytic budding and F-BAR-dependent tubulation in a cell-free system

Min Wu[1,2,4], Bo Huang[5,8,9], Morven Graham[2], Andrea Raimondi[1,2,4], John E. Heuser[7], Xiaowei Zhuang[5,6,8] and Pietro De Camilli[1,2,3,4,10]

Cell-free reconstitution of membrane traffic reactions and the morphological characterization of membrane intermediates that accumulate under these conditions have helped to elucidate the physical and molecular mechanisms involved in membrane transport[1–3]. To gain a better understanding of endocytosis, we have reconstituted vesicle budding and fission from isolated plasma membrane sheets and imaged these events. Electron and fluorescence microscopy, including subdiffraction-limit imaging by stochastic optical reconstruction microscopy (STORM)[4–6], revealed F-BAR (FBP17) domain coated tubules nucleated by clathrin-coated buds when fission was blocked by GTPγS. Triggering fission by replacing GTPγS with GTP led not only to separation of clathrin-coated buds, but also to vesicle formation by fragmentation of the tubules. These results suggest a functional link between FBP17-dependent membrane tubulation and clathrin-dependent budding. They also show that clathrin spatially directs plasma membrane invaginations that lead to the generation of endocytic vesicles larger than those enclosed by the coat.

To gain new insight into mechanisms of endocytosis, we developed a cell-free system suitable for monitoring the formation and progression of endocytic intermediates live at high resolution. Glass-attached plasma membrane sheets, left behind by sonication of fibroblasts grown on coverslips coated with poly-D-lysine, were used as templates to reconstitute cytosol-dependent membrane budding. Sheets were visualized by fluorescence microscopy, either by using cells expressing plasma membrane targeted GFP (PM–GFP) or by a brief incubation with the lipid dye Bodipy-Texas Red Ceramide (BTR) after lysis.

Sheets kept in cytosolic buffer showed a diffuse and rather homogeneous fluorescence, with only a few sparse puncta (Fig. 1a). Within minutes of incubation at 37 °C with brain cytosol, ATP and the non-hydrolysable GTP analogue GTPγS, numerous fluorescence spots appeared (Fig. 1a; Supplementary Information, Movie 1). Concomitant reduction in the glass-contact area of the sheets suggests that the spots represented membrane invaginations (Supplementary Information, Fig. S1). Approximately 15–32% of the total membrane area was sequestered into these membrane puncta during 15 min incubation (Supplementary Information, Fig. S1).

When the same experiment was performed in the presence of GTP instead of GTPγS, few fluorescent spots were observed at the end of 15 min incubation (Fig. 3d), and shrinkage of the membrane was correspondingly smaller: less than 5% was observed (Supplementary Information, Fig. S1). Neither puncta nor shrinkage of the membrane was seen when sheets were incubated at 37 °C with nucleotides but no cytosol.

To test if the fluorescent puncta were related to clathrin-coated pits, the cytosol was supplemented with Alexa555-labelled clathrin. A near-complete coincidence between fluorescent membrane puncta and clathrin was observed (Fig. 1b). These membrane puncta also incorporated classical coated pit cargo, as shown by using membrane sheets derived from cells expressing one such cargo, pHluorin-tagged transferrin receptor (Fig. 1b). Clustering of transferrin receptors increased after incubation with cytosol, ATP and GTPγS (Fig. 1c; Supplementary Information, Movie 2), and fluorescence in the remaining portion of the sheets decreased (Supplementary Information, Fig. S2). Furthermore, sites of transferrin receptor clustering colocalized completely with clathrin puncta (Fig. 1b), indicating that they are sites of clathrin-coated pit nucleation.

To determine the ultrastructure of plasma membrane invaginations, three-dimensional stochastic optical reconstruction microscopy (3D-STORM) and electron microscopy were performed. 3D-STORM is a super-resolution fluorescence microscopy technique with a spatial resolution of 20 nm in the *x*/*y* direction and 50 nm in the *z* direction[6]. For this technique, PM–GFP-labelled sheets were incubated with cytosol, ATP and GTPγS for 15 min, then fixed, labelled with antibodies directed against

[1]Howard Hughes Medical Institute, Yale University School of Medicine, New Haven, CT 06520, USA. [2]Department of Cell Biology, Yale University School of Medicine, New Haven, CT 06520, USA. [3]Department of Neurobiology, Yale University School of Medicine, New Haven, CT 06520, USA. [4]Program in Cellular Neuroscience, Neurodegeneration and Repair, Yale University School of Medicine, New Haven, CT 06520, USA. [5]Department of Chemistry and Chemical Biology, Harvard University, Cambridge MA 02138, USA. [6]Department of Physics, Harvard University, Cambridge MA 02138, USA. [7]Department of Cell Biology and Physiology, Washington University School of Medicine, 660 South Euclid Avenue, St. Louis, MO 63110, USA. [8]Howard Hughes Medical Institute, Harvard University, Cambridge MA 02138, USA.
[9]Current address: Department of Pharmaceutical Chemistry, Department of Biochemistry and Biophysics, University of California, San Francisco, CA 94158, USA.
[10]Correspondence should be addressed to P.D.C. (e-mail: pietro.decamilli@yale.edu)

Received 16 December 2009; accepted 29 July 2010; published online 22 August 2010; corrected online 31 August 2010; DOI: 10.1038/ncb2094

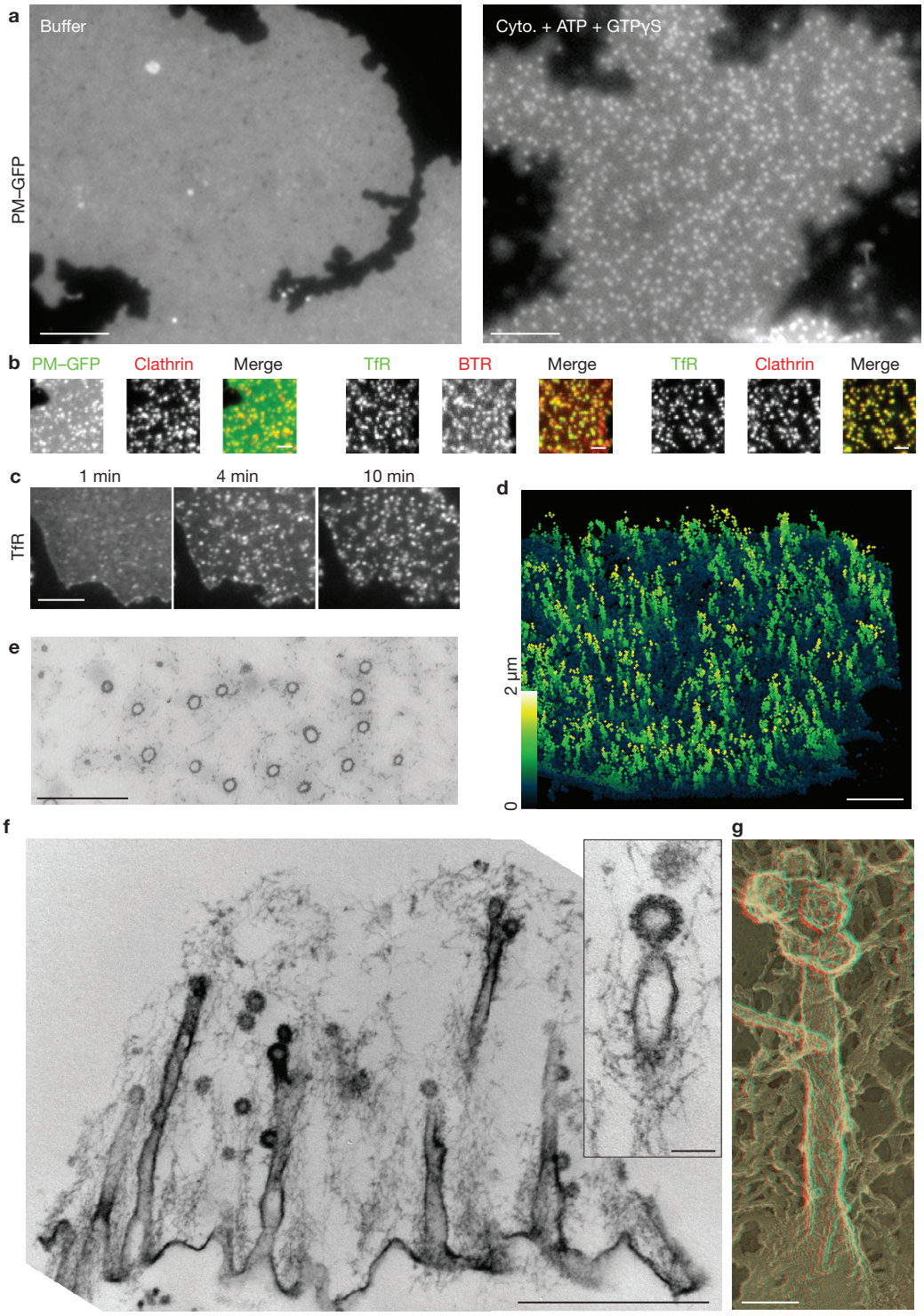

Figure 1 Marked transformation of plasma membrane sheets induced by incubation with brain cytosol. (**a**) Plasma membrane sheets labelled with PM–GFP seem homogeneous without cytosol treatment but become punctate after 15 min incubation with cytosol (Cyto), ATP and GTPγS (see also Supplementary Information, Movie 1). (**b**) Membrane puncta that accumulate on plasma membrane sheets endogenously labelled with PM–GFP or exogenously labelled with the fluorescent lipid marker BTR colocalize with clathrin (Alexa 555-labelled clathrin heavy chain) or transferrin receptor-pHluorin (TfR) puncta. (**c**) Time sequence of transferrin receptor-pHluorin clustering (see Supplementary Information, Movie 2). (**d**) 3D-STORM reconstruction of the transformed plasma membrane. Membrane sheets labelled with PM–GFP were incubated with cytosol, ATP and GTPγS for 15 min, fixed and labelled with anti-GFP, followed by secondary antibody (see Supplementary Information, Movie 3). The colour of individual points in the image encodes distance from the substrate. (**e**) Circular membrane profiles in *en face* thin sections demonstrating the tubular nature of the invaginations. (**f**) Thin section cut perpendicular to the substrate showing longitudinal view of the deep tubular structures that are connected with clathrin-coated pits via constricted necks. Inset is a magnified image of a coated pit at the tip of a tubular structure. (**g**) Electron microscopy of the platinum replica of quick-frozen deep-etched membrane sheet illustrating deep tubular extensions capped with multiple clathrin-coated pits. Samples in **e**–**g** were incubated with cytosol, ATP and GTPγS for 15 min. Scale bars, 5 µm (**a**); 2 µm (**b**); 5 µm (**c**); 2 µm (**d**); 1 µm (**e**); 1 µm (**f**); 100 nm (**f**, inset; **g**).

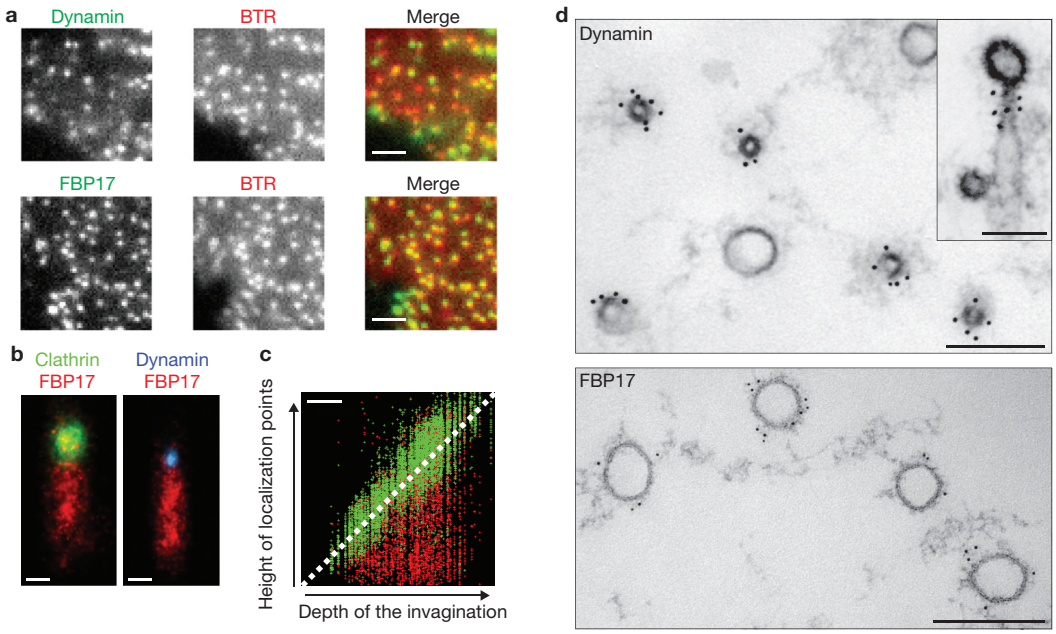

Figure 2 Localization and axial segregation of dynamin and FBP17 along the tubular invaginations. (**a**) Alexa488 dynamin and Alexa 488 FBP17 were both recruited to the membrane invaginations as indicated by fluorescence lipid puncta (BTR). (**b**) Stacked 3D-STORM images of 59 membrane invaginations labelled with FBP17 (immunofluorescence with Cy3–Cy5-labelled secondary antibodies) and aligned according to the position of the coat region (Alexa 405-Cy5-labelled clathrin heavy chain), and of 96 membrane invaginations aligned according to the position of the constriction site where dynamin (Alexa 405–Cy5-labelled dynamin) was localized. (**c**) The distribution of clathrin and FBP17 along the length of tubules as a function of the depth of invaginations. The *x*-*z* 3D-STORM images of 207 membrane invaginations labelled with FBP17 (immunofluorescence with Cy3/Cy5-labelled secondary antibodies) and clathrin (Alexa 405–Cy5 labelled clathrin heavy chain) were used to generate this scatter plot. Clathrin localization points follow the diagonal line as expected, whereas FBP17 points fill the space underneath the clathrin structure regardless of the depth of the invagination. (**d**) Immunogold localization of FBP17 and dynamin (polyclonal antibody DG1) on cross-sections of the tubular invaginations. The top section captured a plane closer to the tip of the tubules. Inset shows a side view. All samples in Fig. 2 were prepared by incubating membrane sheets with cytosol, ATP and GTPγS for 15 min then fixed. Scale bars, 2 μm (**a**); 200 nm (**b**–**d**);

GFP, and secondary antibodies conjugated with the photo-switchable dye pair Alexa405–Cy5. Reconstructed STORM images show that the fluorescence membrane puncta, observed by conventional fluorescence microscopy, were in fact highly elongated structures perpendicular to the surface (Fig. 1d; Supplementary Information, Movie 3).

Thin-section electron microscopy, as well as deep-etch electron microscopy of platinum replica, complemented these observations by revealing a substantial presence of deep, tubular plasma membrane invaginations (Fig. 1e–g), which were always capped by one or several small clathrin-coated pits (diameter approximately 50–70 nm). Occasionally, clathrin-coated pits were also localized along the tubules. Most of the tubules had a diameter of 57 ± 6 nm. Typically, they tapered sharply at their tips, with a constriction at the boundary between the tubules and the coated pits (30–40 nm), and were often larger at their base next to the glass substrate (80–120 nm). Control plasma membranes incubated with cytosolic buffer alone revealed few features other than some membrane undulation and occasional clathrin-coated pits that were present before lysis. Cytosol plus ATP and GTP enhanced the number of clathrin-coated pits, but in both conditions the marked tubulation was absent (Fig. 3c). Note that in both of these conditions, the PM–GFP fluorescence signal remained roughly homogenous (Figs 1a, 3d). Thus, the invagination produced by a typical clathrin-coated pit is not sufficient to generate a significantly higher membrane fluorescence signal relative to the surrounding membrane; under our experimental conditions, fluorescent membrane puncta are in fact reporters of deep membrane invaginations.

To gain insight into the molecular nature of the tubules, we explored whether tubulating proteins with putative roles in endocytosis might be present on these structures. Addition of fluorescently labelled dynamin[7], endophilin (a BAR protein)[8] and FBP17 (an F-BAR protein of the FBP17/CIP4/Toca1 family)[9–11] to the cytosol showed that all these proteins were recruited to the sites of membrane invagination (Fig. 2a; Supplementary Information, Fig. S3). However, although these proteins were localized to the same puncta in the *x*, *y* dimension, close examination in *z* stacks revealed segregation of these proteins along the axial direction of the tubules (Supplementary Information, Fig. S3). Dynamin colocalized precisely with endophilin both in the *x*, *y* dimension and in the *z* dimension. By contrast, dynamin and endophilin overlapped only partially with FBP17 in the *z* direction, being concentrated at the tip of the tubules.

Stacked 3D-STORM images of membrane invaginations labelled for clathrin (clathrin heavy chain directly labelled with Alexa 405-Cy5) and FBP17 (immunostained with Cy3–Cy5-labelled secondary antibodies) further demonstrated that FBP17 was present along the entire length of the large tubules (Fig. 2b, c), whereas dynamin (directly labelled with Alexa 405-Cy5) was localized in the neck between the coated pit and the FBP17-coated tubules (Fig. 2b). Accordingly, immunogold labelling of *en face* thin sections revealed that FBP17 was localized on the wide portions of the tubules. These tubules had diameters between 50 nm and 120 nm (Fig. 2d), which is the same size range of tubules generated by FBP17 when overexpressed in cells or incubated *in vitro* with liposomes[10,12]. Dynamin localized exclusively to the narrow tubular necks linking wide

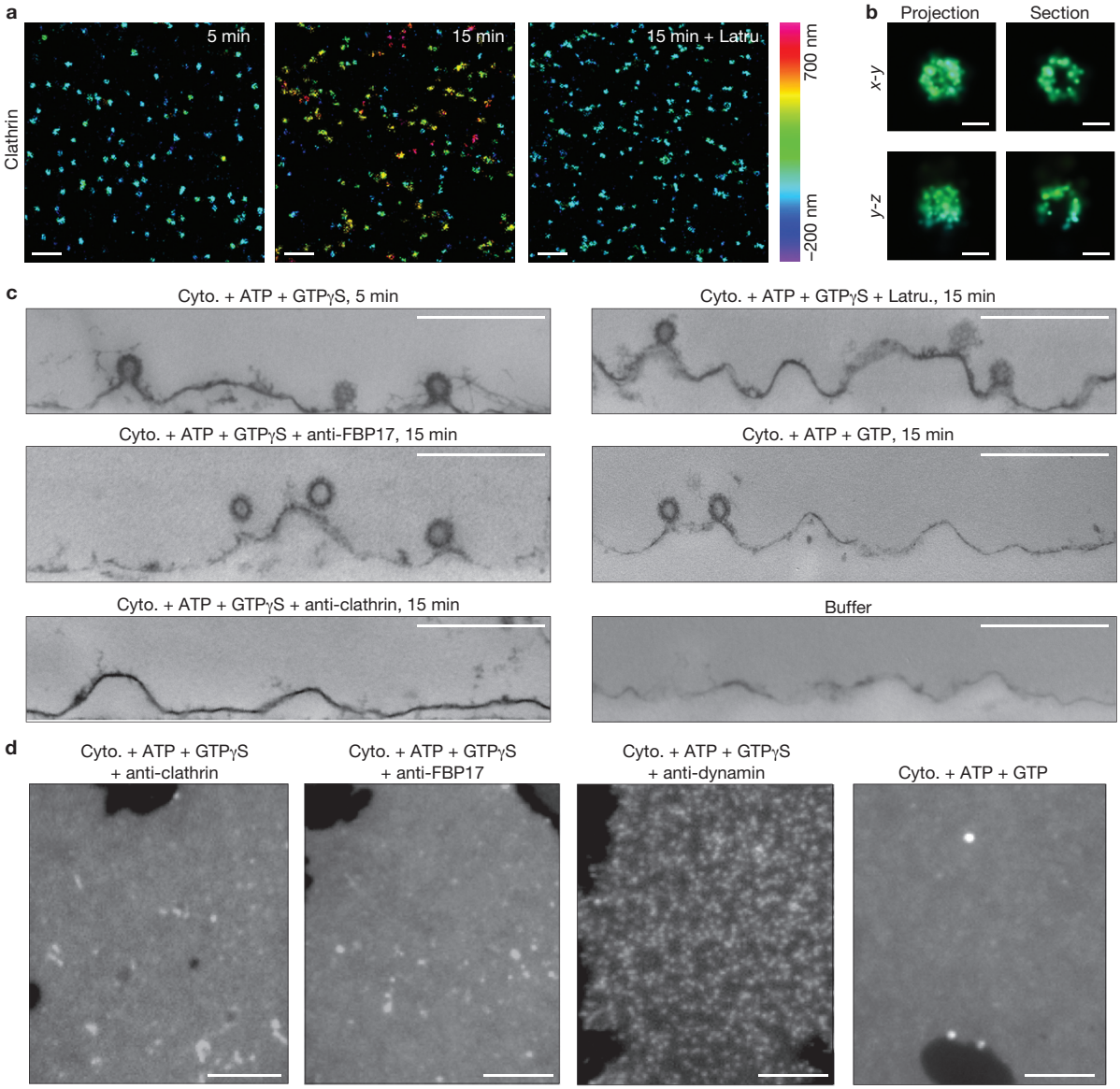

Figure 3 Tubular invaginations require spatially coordinated action of clathrin, actin and FBP17. (**a**) 3D-STORM images of clathrin (Alexa 405-Cy5-labelled clathrin heavy chain) at different time points after incubation with cytosol, ATP plus GTPγS, and in the absence or presence of latrunculin B (Latru). Two-colour 3D imaging was performed together with PM–GFP (not shown here). (**b**) High-magnification view of 3D-STORM images of a single clathrin-coated pit. In the right panels, the horizontal and vertical projections of the 3D image of one clathrin structure shows the half-spherical shape of the pit, whereas 50-nm thick cross-sections through the geometric centre of the pit reveals that inside is hollow (in both *x-y* and *y-z* views) and there is an opening at the bottom (only in *y-z* view), as expected for clathrin-coated pits. In both **a** and **b**, the colour of individual points in the images encodes distance from the mean height of the basal membrane sheet. (**c**) Thin-section electron microscopy confirms the presence of clathrin-coated pits, but a lack of tubulation at the early point (5 min) of incubation with cytosol, ATP plus GTPγS, or at later time point (15 min) in the presence of latrunculin B, anti-FBP17 antibodies, or GTP instead of GTPγS. In the absence of cytosol or in the presence of anti-clathrin antibodies, clathrin-coated pits are rare. (**d**) Fluorescence images of plasma membrane sheets (labelled with PM–GFP) after incubations as indicated. Scale bars, 1 μm (**a**); 100 nm (**b**); 500 nm (**c**); 5 μm (**d**).

tubules to the clathrin-coated buds (Fig. 2d). The diameters of these neck regions are 35 ± 5 nm, consistent with the diameter of dynamin-coated or endophilin-coated tubules[13,14].

We next analysed the temporal sequence of clathrin recruitment and tubule elongation. The distance between the clathrin signal and the PM–GFP-labelled basal membrane was imaged by 2-colour 3D-STORM at different time points after the cytosol and nucleotides were added. Formation of clathrin-coated pits had already occurred at 5 min, with 2.1 ± 0.3 pits per μm^2 (Fig. 3a, b, only the clathrin signals are shown). At this time they were located close to the basal membrane, with a mean distance of 90 ± 61 nm (Fig. 3a; Supplementary Information, Fig. S4). At 15 min, they had risen to a mean distance of 371 ± 204 nm from the basal membrane with 2.0 ± 0.3 pits per μm^2 (Fig. 3a; Supplementary Information, Fig. S4). Thin-section electron microscopy confirmed the assembly of clathrin-coated pits and their location next to the bottom surface at 5 min (Fig. 3c). Thus, under these cell-free conditions, recruitment of clathrin precedes tubule growth, suggesting that clathrin is needed to spatially guide tubular growth.

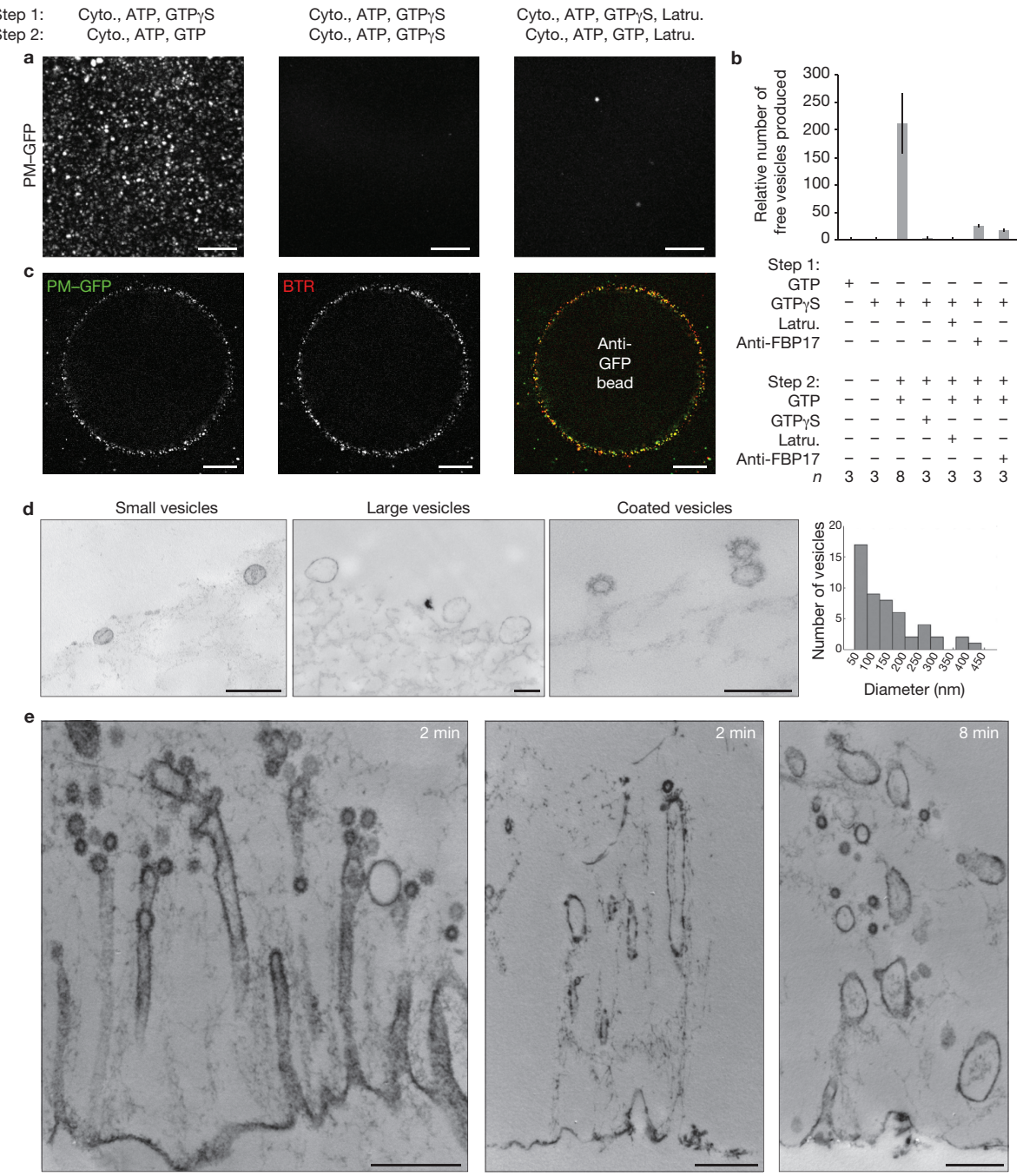

Figure 4 Occurrence of membrane fission on replacement of GTPγS with GTP. (**a**) Appearance of free vesicles (labelled with PM–GFP) in the medium in the presence of GTP, but not in the continued presence of GTPγS or latrunculin B. Each image is the maximum intensity projection of 50 frames by confocal microscopy (see also Supplementary Information, Movie 4). (**b**) Quantification of the number of free vesicles formed under various incubation conditions. The number for each condition was obtained by counting the mean number of vesicles per frame. Data represent means ± s.e.m. (*n* values are indicated at the bottom). (**c**) Immunocapture of vesicles (PM–GFP positive) on beads coated with anti-GFP antibodies and colocalization with a membrane marker (BTR; see Supplementary Information, Movie 5). (**d**) Electron microscopy of bead-bound vesicles and distribution of their diameters. (**e**) Electron microscopy of plasma membrane sheets at various times after replacement of GTPγS with GTP. Scale bars, 10 μm (**a**); 20 μm (**c**); 200 nm (**d**); 500 nm (**e**).

When antibodies that block clathrin polymerization were included in the cytosol, membrane sheets remained roughly flat, indicating a lack of tubulation (Fig. 3d). This was further confirmed by electron microscopy (Fig. 3c). The absence of deep invaginations, despite the presence of abundant tubulating proteins in the cytosol, suggests that formation of clathrin-coated pits is not only needed to spatially direct tubular growth, but also to trigger tubular growth itself. Pre-incubation of cytosol with anti-FBP17 antibodies also strongly inhibited plasma membrane tubulating activity (Fig. 3c, d), consistent with a strong presence of this protein in the wide tubular portion. By contrast, antibodies directed against

dynamin did not prevent membrane tubulation, as indicated by the accumulation of fluorescence membrane puncta (Fig. 3d).

In the presence of latrunculin B (125 μM), which blocks actin polymerization, clathrin-coated pits accumulated on the membrane sheets (2.3 ± 0.2 pits per μm^2) to a similar extent as in the absence of the drug, but they remained close to the basal membrane with a mean distance of 79 ± 39 nm (Fig. 3a; Supplementary Information, Fig. S4). Accordingly, electron microscopy showed that the tubules were absent under these conditions (Fig. 3c). Many endocytic proteins, including proteins with robust tubulating activity such as FBP17, are intimately linked to actin polymerization[11,15,16]. These results suggest that a synergistic action of actin and tubulating proteins is required for the formation of tubular invaginations in response to clathrin-coated pits nucleation (similar results were recently reported in a system involving clathrin-dependent formation of tubular intermediates on giant unilamellar liposomes[17]). Interestingly, addition of latrunculin B (125 μM) to the membrane sheets after tubules had already formed led to loss of the actin cytoskeleton while tubules persisted (Supplementary Information, Fig. S5a, b). This observation suggests that, during tubulation, actin facilitates the assembly around the tubules of a stabilizing scaffold containing an F-BAR domain. Intermolecular interactions within such a scaffold may then contribute[12], at least in part, to tubule stability after actin disassembly, as supported by the slow turnover rate of FBP17 on the tubules revealed by FRAP (Supplementary Information, Fig. S5c, d).

Importantly, under all conditions where clathrin-coated pits assembled but wide tubules were absent, including in the presence of anti-FBP17 antibodies, the necks of clathrin-coated pits were constricted to a diameter below that of the large tubules (Fig. 3c). Thus, neck constriction and wide tubular growth are probably independently regulated processes, with the latter more dependent on FBP17.

Finally, to determine whether fission could occur in our cell-free system, and whether tubular invaginations are important for this reaction, we monitored by fluorescence the appearance of free vesicles formed from PM–GFP-labelled membrane sheets and their recovery on Sepharose beads coated with anti-GFP antibodies. Generation of free vesicles was virtually absent in the single incubation with cytosol, ATP plus GTPγS or GTP (Fig. 4b). However, when cytosol plus ATP and GTP were added to the intermediates generated by a first incubation with cytosol, ATP and GTPγS, a large number of free vesicles was observed in the medium within minutes (Fig. 4a, b; Supplementary Information, Movie 4). These newly formed vesicles could be captured with minimal mechanical perturbation by addition of beads coated with anti-GFP antibodies, together with the second incubation mixture (Fig. 4c), but not by control beads devoid of specific antibodies (Supplementary Information, Fig. S6). PM–GFP puncta on the beads colocalized precisely with the fluorescent membrane marker BTR (Fig. 4c; Supplementary Information, Movie 5), confirming their membrane nature.

Thin-section electron microscopy of the material recovered on the beads demonstrated the presence of small 40–70 nm coated and uncoated vesicles, as well as of larger vesicles of 100–400 nm (Fig. 4d). A corresponding loss of tubular invaginations replaced by vesicular structures was observed on the membrane sheets (Fig. 4e). These findings demonstrate the occurrence of fission and suggest that both clathrin-coated pits and tubular regions serve as precursors of free vesicles. The small vesicles are probably derived from the coated pits and the large vesicles probably arise from the large tubular region. No free vesicles were observed when GTPγS or latrunculin B were included in both incubations (Fig. 4a, b). Antibodies directed against FBP17 did not completely abolish, but significantly inhibited vesicle formation when added to either incubation (Fig. 4b).

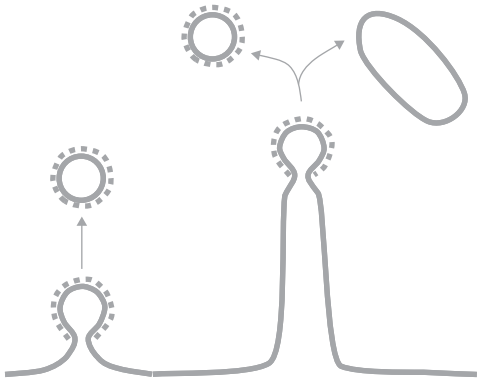

Figure 5 Schematic representation of the membrane invaginations described in this study and of their fission. The model illustrates how an endocytic reaction triggered by clathrin may lead to both classical clathrin-coated vesicles derived from the coated bud and non-coated larger vesicles derived from the tubular region.

Collectively, our results provide a striking demonstration of the hypothesis that membrane tubulation factors present in the cytosol are linked to endocytosis. FBP17 is one such factor, thus supporting an endocytic function of the FBP17/CIP4/Toca family, as previously suggested by functional[10,11,18] and genetic studies[19]. Our results further reveal a robust relationship between clathrin-coated pits and FBP17-mediated tubulation. FBP17 was reported to be recruited to clathrin-coated pits in living fibroblasts[18]. The shallow curvature of the membrane-binding surface of its F-BAR domain led to the hypothesis that FBP17 and other members of the FBP17/CIP4/Toca1 family may function before the final constriction of the pits[18], a process probably regulated by BAR-domain proteins with a sharper curvature, such as amphiphysin[20], endophilin[8,21] and SNX9 (ref. 22). An even earlier action was recently demonstrated for FCHo, another F-BAR-domain containing protein[23]. FCHo is recruited before clathrin assembly and dissociates from clathrin-coated pits as they mature, and thus was proposed to nucleate them[23]. This function is unlikely to be generally applicable to other F-BAR proteins, as it is the carboxy-terminal region of FCHo, the μ homology domain, which has a key role in its localization to clathrin-coated pits. F-BAR proteins of the FBP17/CIP4/Toca1 family, which contain a C-terminal SH3 domain instead of the μ homology domain, are recruited later to clathrin-coated pits[18,23]. Importantly, FBP17 is not an essential component of clathrin-coated pits *in vivo*, as it is not recruited to every clathrin-coated pit in non-neuronal cells[23], and the triple knockdown of FBP17/CIP4/Toca1 has only a partial inhibitory effect on transferrin uptake[10]. Our findings are consistent with FBP17-mediated tubulation acting after (or in parallel with) maturation of the pits, and independently contributing to membrane dynamics at the endocytic site, for example by regulating the extent of membrane internalized (Fig. 5).

As in the case for all cell-free systems, the system that we have described does not precisely recapitulate conditions occurring in a living cell. However, it uses a natural plasma-membrane template and cytosol, and thus closely mimics the physiological environment. Hence, coordination of clathrin-mediated budding with the formation of F-BAR-domain-coated tubules observed in this study probably reflects

physiologically relevant phenomena. In live cells, membrane tubulation is expected to be antagonized by membrane tension[24,25]. Membrane sheets prepared here represent a lower tension membrane template and may thus facilitate the production of tubular intermediates by FBP17, which may act as a tension sensor. The prominence of such tubules will be further enhanced by an inhibition in fission activity. For example, elongated tubular intermediates capped by clathrin-coated pits with similar diameter to those described in this study have been observed in garland cells of *shibire*, a temperature-sensitive mutant of dynamin[26]. Nevertheless, similar intermediates have also been seen in wild-type cells[27,28]. The appearance of such intermediates may result from a transient shift in the balance between tubulation and fission activity caused by regulatory mechanisms *in vivo*. In addition, unconventional roles of clathrin in endocytosis have been described previously[29], and in some cases the endocytic reaction results in the internalization of plasma membrane fragments that are larger than the vesicle scaffolded by the clathrin coat itself[30]. Taken together, our study provides strong support for the importance of F-BAR-dependent tubular endocytic intermediates in endocytosis, and reveals new endocytic intermediates that might correspond to a physiological stage of endocytosis. The generation of large membrane fragments from the plasma membrane sheets can be considered a form of clathrin-dependent bulk endocytosis. Thus, our study also demonstrates the possibility of using a cell-free system to study this still mechanistically elusive endocytic reaction. □

ACKNOWLEDGEMENTS

We thank Aurelien Roux and Yuxin Mao for advice and help; Lijun Liu, Frank Wilson and Christoph Rahner for critical technical assistance. This work was supported in part by the G. Harold and Leila Y. Mathers Charitable Foundation, the W.M. Keck Foundation and the National Institutes of Health grants (NS36251 and DK45735) to P.D.C., and National Institutes of Health grant (GM068518) to X.Z.; P.D.C. and X.Z. are Howard Hughes Medical Institute Investigators.

AUTHOR CONTRIBUTIONS

M.W. and P.D.C. designed the experiments and wrote the manuscript; M.W. performed experiments. Experimental work was also contributed by B.H. (STORM), J.E.H. (electron microscopy), A.R. (electron microscopy) and M.G. (electron microscopy). B.H. and X.Z. also contributed to discussion and manuscript preparation.

COMPETING INTERESTS

The authors declare no competing financial interests.

Published online at http://www.nature.com/naturecellbiology
Reprints and permissions information is available online at http://npg.nature.com/reprintsandpermissions/

1. Moore, M., Mahaffey, D., Brodsky, F. & Anderson, R. Assembly of clathrin-coated pits onto purified plasma membranes. *Science* **236,** 558–563 (1987).
2. Smythe, E., Pypaert, M., Lucocq, J. & Warren, G. Formation of coated vesicles from coated pits in broken A431 cells. *J. Cell Biol.* **108,** 843–853 (1989).
3. Schmid, S. L. & Smythe, E. Stage-specific assays for coated pit formation and coated vesicle budding *in vitro*. *J. Cell Biol.* **114,** 869–880 (1991).
4. Rust, M. J., Bates, M. & Zhuang, X. Sub-diffraction-limit imaging by stochastic optical reconstruction microscopy (STORM). *Nat. Methods* **3,** 793–796 (2006).
5. Bates, M., Huang, B., Dempsey, G. T. & Zhuang, X. Multicolor Super-Resolution Imaging with Photo-Switchable Fluorescent Probes. *Science* **317,** 1749–1753 (2007).
6. Huang, B., Wang, W., Bates, M. & Zhuang, X. Three-dimensional super-resolution imaging by stochastic optical reconstruction microscopy. *Science* **319,** 810–813 (2008).
7. Hinshaw, J. E. Dynamin and its role in membrane fission. *Annu. Rev. Cell Dev. Biol.* **16,** 483–519 (2000).
8. Farsad, K. *et al.* Generation of high curvature membranes mediated by direct endophilin bilayer interactions. *J. Cell Biol.* **155,** 193–200 (2001).
9. Kamioka, Y. *et al.* A novel dynamin-associating molecule, formin-binding protein 17, induces tubular membrane invaginations and participates in endocytosis. *J. Biol. Chem.* **279,** 40091–40099 (2004).
10. Itoh, T. *et al.* Dynamin and the actin cytoskeleton cooperatively regulate plasma membrane invagination by BAR and F-BAR proteins. *Dev. Cell* **9,** 791–804 (2005).
11. Tsujita, K. *et al.* Coordination between the actin cytoskeleton and membrane deformation by a novel membrane tubulation domain of PCH proteins is involved in endocytosis. *J. Cell Biol.* **172,** 269–279 (2006).
12. Frost, A. *et al.* Structural basis of membrane invagination by F-BAR domains. *Cell* **132,** 807–817 (2008).
13. Takei, K., McPherson, P. S., Schmid, S. L. & Camilli, P. D. Tubular membrane invaginations coated by dynamin rings are induced by GTP-γS in nerve terminals. *Nature* **374,** 186–190 (1995).
14. Ringstad, N. *et al.* Endophilin/SH3p4 is required for the transition from early to late stages in clathrin-mediated synaptic vesicle endocytosis. *Neuron* **24,** 143–154 (1999).
15. Ho, H.-Y. H. *et al.* Toca-1 mediates Cdc42-dependent actin nucleation by activating the N-WASP-WIP complex. *Cell* **118,** 203–216 (2004).
16. Takano, K., Toyooka, K. & Suetsugu, S. EFC/F-BAR proteins and the N-WASP-WIP complex induce membrane curvature-dependent actin polymerization. *EMBO J.* **27,** 2817–2828 (2008).
17. Anitei, M. *et al.* Protein complexes containing CYFIP/Sra/PIR121 coordinate Arf1 and Rac1 signalling during clathrin-AP-1-coated carrier biogenesis at the TGN. *Nat. Cell Biol.* **12,** 330–340 (2010).
18. Shimada, A. *et al.* Curved EFC/F-BAR-domain dimers are joined end to end into a filament for membrane invagination in endocytosis. *Cell* **129,** 761–772 (2007).
19. Giuliani, C. *et al.* Requirements for F-BAR proteins TOCA-1 and TOCA-2 in actin dynamics and membrane trafficking during *Caenorhabditis elegans* oocyte growth and embryonic epidermal morphogenesis. *PLoS Genet.* **5,** e1000675 (2009).
20. Takei, K., Slepnev, V. I., Haucke, V. & De Camilli, P. Functional partnership between amphiphysin and dynamin in clathrin-mediated endocytosis. *Nat. Cell Biol.* **1,** 33–39 (1999).
21. Ferguson, S. *et al.* Coordinated actions of actin and BAR proteins upstream of dynamin at endocytic clathrin-coated pits. *Dev. Cell* **17,** 811–822 (2009).
22. Soulet, F., Yarar, D., Leonard, M. & Schmid, S. L. SNX9 regulates dynamin assembly and is required for efficient clathrin-mediated endocytosis. *Mol. Biol. Cell* **16,** 2058–2067 (2005).
23. Henne, W. M. *et al.* FCHo proteins are nucleators of clathrin-mediated endocytosis. *Science* **328,** 1281–1284 (2010).
24. Sheetz, M. P. & Dai, J. Modulation of membrane dynamics and cell motility by membrane tension. *Trends Cell Biol.* **6,** 85–89 (1996).
25. Zimmerberg, J. & Kozlov, M. M. How proteins produce cellular membrane curvature. *Nat. Rev. Mol. Cell Biol.* **7,** 9–19 (2006).
26. Kosaka, T. & Ikeda, K. Reversible blockage of membrane retrieval and endocytosis in the garland cell of the temperature-sensitive mutant of *Drosophila melanogaster*, shibirets. *J. Cell Biol.* **97,** 499–507 (1983).
27. Willingham, M. *et al.* Receptor-mediated endocytosis in cultured fibroblasts: cryptic coated pits and the formation of receptosomes. *J. Histochem. Cytochem.* **29,** 1003–1013 (1981).
28. He, W. *et al.* FcRn-mediated antibody transport across epithelial cells revealed by electron tomography. *Nature* **455,** 542–546 (2008).
29. Veiga, E. *et al.* Invasive and adherent bacterial pathogens co-opt host clathrin for infection. *Cell Host Microbe* **2,** 340–351 (2007).
30. Cureton, D. K., Massol, R. H., Saffarian, S., Kirchhausen, T. L. & Whelan, S. P. J. Vesicular stomatitis virus enters cells through vesicles incompletely coated with clathrin that depend upon actin for internalization. *PLoS Pathog.* **5,** e1000394 (2009).

METHODS

Reagents. Antibodies to clathrin heavy chain (X22, Affinity Bioreagents), dynamin (clone 41, BD transduction), GFP (rabbit IgG, Invitrogen) and gold-conjugated (12-nm or 6-nm particles, Jackson ImmunoResearch) anti-rabbit antibodies were purchased commercially. Polyclonal antibodies to dynamin (DG1) for immunogold localization were generated by our lab and described previously[31]. Polyclonal antibodies to FBP17 for immunogold and STORM localization were generated by our lab and described previously[10]. Fluorescent lipid BODIPY TR ceramide (BTR) was purchased from Invitrogen. Rhodamine skeletal muscle actin was purchased from Cytoskselton. All other chemicals were from Sigma.

Cytosol. Adult mouse brains were homogenized in breaking buffer (25 mM Tris pH 8.0, 500 mM KCl, 250 mM sucrose, 2 mM EGTA, 1 mM dithiothreitol (DTT)) in the presence of a protease inhibitor cocktail (Roche). The lysate was centrifuged at 160,000*g* for 2 h and the resulting supernatant was desalted on PD-10 (Amersham Biosciences) at room temperature into cytosolic buffer (25mM Hepes pH 7.4, 120 mM potassium glutamate, 20 mM potassium chloride, 2.5 mM magnesium acetate, 5 mM EGTA). Aliquots of cytosol were frozen in liquid nitrogen and stored at −80 °C for up to 2 months.

Purified proteins and their conjugation to fluorophores. The following commercial fluorophores were used in protein conjugations: Alexa 488 maleimide (Invitrogen A10254), Alexa 555 maleimide (Invitrogen A20346), Alexa 594 maleimide (Invitrogen A10256). Covalently linked activator-reporter pairs Alexa 405-Cy5 maleimide were prepared as described previously[32].

Clathrin was purified from bovine brains, as described previously[33]. To conjugate clathrin with fluorescent dyes, clathrin was reacted with the dyes (Alexa 405-Cy5 or Alexa 555 maleimide, dye protein molar ratio 8) at room temperature for 30 min. One round of polymerization and depolymerization was done to remove non-functional clathrin or aggregates. Briefly, the reaction product was dialysed into polymerization buffer (40 mM NaMES pH 6.5, 3 mM $CaCl_2$, 0.5 mM $MgCl_2$, 1 mM EGTA, 1 mM DTT) overnight at 4 °C. The solution was centrifuged at 150,000*g* for 1 h and the resulting pellet was resuspended into depolymerization buffer (20 mM TrisHCl pH 7.8, 1 mM EDTA) and dialysed into the same buffer overnight at 4 °C. After centrifugation at 150,000*g* for 1 h, the supernatant was collected and dialysed into storage buffer (20 mM Hepes pH 7.4, 120 mM NaCl, 1 mM DTT).

Dynamin was purified from rat brains and conjugated with fluorescent dyes (Alexa 488 maleimide, Alexa405-Cy5 maleimide) as described previously[34]. FBP17 was purified as GST fusion protein as described previously[10]. After cleavage of the GST tag, FBP17 was conjugated to Alexa 488 maleimide (Invitrogen A10254) by reacting with the dye (dye protein molar ratio 4) at room temperature for 30 min. The final product was dialysed into a high salt storage buffer (20 mM Hepes pH 7.4, 300 mM NaCl, 1 mM DTT).

Membrane sheets. PTK2 cells were maintained at 37 °C in 10% CO_2 in minimum essential Eagle medium (Invitrogen) supplemented with 10% (v/v) fetal bovine serum, 100 μg ml^{-1} penicillin/streptomycin. PTK2 cells stably expressing PM–GFP[35], transferrin receptor-phluorin[36] were maintained with 0.5mg ml^{-1} G418. To prepare membrane sheets[37–39], cells were grown for 24-48 h until confluent in MatTek dishes (MatTek) that had been coated with 20 μg ml^{-1} poly-D-lysine for 30 min and washed overnight. They were sheared in ice-cold cytosolic buffer (25 mM Hepes at pH 7.4, 120 mM potassium glutamate, 20 mM potassium chloride, 2.5 mM magnesium acetate, 5 mM EGTA and 1 mM DTT) by a brief pulse of sonication (about 1 s) using a cell disruptor (VirTis Ultrasonics) set at 15–17% of output power with a 1/8-inch microprobe positioned at about 15 mm above the dish. After shearing, membrane sheets were rinsed in cytosolic buffer and used for the *in vitro* assay within 20 min. When a fluorescent lipid marker was used to visualize the membrane, membrane sheets were incubated with 5 μM BTR at 37 °C for 5 min and rinsed to remove excess dyes.

***In vitro* assay.** Membrane sheets were incubated at 37 °C with cytosol and nucleotides as indicated. The final concentration of cytosol and nucleotides was as follows: cytosol, 4mg ml^{-1}; ATP, 1.5 mM; GTPγS, 150 μM; GTP, 1.6 mM. Samples containing ATP were supplemented with an ATP-regenerating system consisting of 16.7 mM creatine phosphate and 16.7 U ml^{-1} creatine phosphokinase[20]. Samples containing GTP were supplemented with a GTP-regenerating system consisting of 1 mM phosphopyruvate and 20 U ml^{-1} pyruvate kinase. Fluorescent proteins added to the cytosol were used at the following concentrations: clathrin, 500 nM; dynamin, 125 nM; FBP17, 50–250 nM. When indicated, cytosol was pre-incubated with anti-clathrin (0.5 mg ml^{-1}), anti-dynamin (50 μg ml^{-1}) or anti-FBP17 (20 μg ml^{-1}) at 4 °C for 1–2 h. Heat denatured antibodies were used as negative controls. In real-time imaging, an oxygen-scavenging system (4.5 mg ml^{-1} glucose, 1.25 μM glucose oxidase, 140 nM catalase, 71.5 mM 2-mercaptoethanol) was included. For the two-step fission assay, membrane sheets were incubated with a dose of cytosolic mixture for 15–20 min, washed with cytosolic buffer and incubated with second dose of cytosolic mixture. For immunocapture of the fissioned vesicles, protein A Sepharose CL-4B beads (GE Healthcare) were coated with anti-GFP (0.4 mg ml^{-1}) at 4 °C for 1 h, washed in cytosolic buffer, and added together with second dose of cytosolic mixture at a volume ratio of 1:10.

Fluorescence microscopy and image analysis. Epifluorescence imaging was done using a Leica DMI6000 inverted microscopy equipped with CCD camera (Coolsnap HQ) and temperature controlled chamber. A mercury lamp (EXFO X-Cite 120) or a xenon arc lamp (Lambda DG-4) was used as light source. All images were acquired through either ×63 oil (NA1.3, PL APO) or ×100 oil (NA1.4, PL APO) objectives and the following filter combinations: Ex.: BP 470/40; Dich. 500; Em.: BP 525/50 for green; Ex.: BP 546/12; Dich. 560; Em.: BP 605/75 for red; Ex.: BP 565/55; Dich. 600; Em.: BP 650/75 for far red. Metamorph (Universal Imaging) was used to acquire either single colour image or sequential 2-colour images using binning 2.

Real-time fission assay and FRAP experiments were performed on an UltraVIEW VoX spinning disc confocal (SDC) microscope (Perkin Elmer) equipped with Perfect Focus, temperature controlled stage, EMCCD camera (Hamamatsu C9100-50) and controlled by Volocity software (Improvision). All images were acquired through a ×60 or ×100 oil objective (NA 1.4, CFI Plan Apo VC). Green fluorescence was excited with a 488 nm/50 mW diode laser and collected by a BP 527/55 filter. Red fluorescence was excited with a 561 nm/50 mW diode laser and collected by a BP 615/70 filter. Two-colour images were acquired sequentially. For fluorescence recovery after photobleaching, a region of interest (50 × 50 pixels, 14 μm^2) was chosen on the sheet and the 488 nm/50 mW laser at 100% power was used to bleach this region for 100 cycles. Images were acquired by a ×100 oil objective (NA 1.4, CFI Plan Apo VC) at 10-s intervals and at least 10 frames were acquired before bleaching.

Quantification of fission events was done by counting fluorescence spots in SDC images using custom written algorithm in Matlab. Briefly, for each reaction, a 30-min movie (usually 180 frames), including before and after adding GTP, was acquired at 20 μm above the surface. Median filter was applied to each frame of the image series and local background was subtracted. Vesicles were identified as pixels with local maximum intensity above a fixed threshold. The identified particles were overlaid with original movie for visual inspection. The number of the vesicles per frame (1000 × 1000 pixels, 14,400 μm^2) was plotted against time and fifty frames with highest number of peaks were averaged to give the final number for this reaction. For each condition, three to eight independent experiments were performed, as indicated.

Quantification of FRAP was done by calculating the average intensity of the bleached region, which was corrected with background (average intensity of a non-fluorescent region) and normalized with the average intensity of a neighbouring fluorescent but non-bleached region to account for global intensity changes. The subsequent recovery curve was fitted with the Soumpasis equation

$$F(t) = A \cdot e^{-2T/t} \cdot (I_0(2T/t) + I_1(2T/t)) + B$$

where I_0, I_1 are modified Bessel functions, A, B and T are free parameters that describe the increase in fluorescence intensity after recovery $F(\infty)$–$F(0)$, the fluorescence intensity immediately after bleaching $F(0)$ and the recovery time.

STORM. After the reaction, samples were rinsed and fixed in 4% paraformaldehyde, 0.1% glutaraldehyde and 5 μM phalloidin at room temperature for 20 min. In the case of immunostaining, after incubation with primary (rabbit anti-FBP17: 1:200; rabbit anti-GFP 1:200) and secondary antibody (1:200) for 30 min, samples were fixed for an additional 20 min. Imaging was done as described previously[6,32]. Briefly, super-resolution images were acquired on an Olympus IX-71 inverted microscope equipped with a ×100 NA 1.4 oil immersion objective. Three activation lasers and one imaging laser (CUBE 405-50C and Sapphire 460-10 from

DOI: 10.1038/ncb2094

Coherent, GCL-200-L and RCL-200-656 from Crystalaser) are individually shuttered and illuminate the sample in wide-field high-incident-angle mode. A dichroic mirror (T660LPXR, Chorma) and an emission filter (ET705/70m, Chroma) allows the single-molecule photoactivation events to be captured by an EMCCD camera (Ixon DV897DCS-BV, Andor) through a cylindrical lens that creates an astigmatism for 3D localization. The reflected imaging laser from the bottom of the culture dish was redirected to a quadrant photodiode, providing the feedback signal to a piezo objective positioner (Nano F-100, Madcity Labs) to stabilize the focusing of the microscope. One STORM image consists of 1 to 3 *z*-slices acquired at focal plane positions separated by approximately 470 nm to cover the entire height of the sample, with 5,000–10,000 raw image frames recorded per slice. After correcting for the spherical aberration of refractive index mismatch between the coverglass and imaging buffer[32], each slice covers a *z* range of about 650–900 nm, depending on the distance of the focal plane to the coverglass surface. Crosstalk between colour channels was subtracted statistically.

Electron microscopy. Samples were fixed in 2.5% glutaraldehyde containing 1% tannic acid for 1 h at room temperature, rinsed 3 times in cytosolic buffer, stained in 1% osmium tetroxide in phosphate buffer (100 mM sodium phosphate, 50 mM KCl, 5 mM $MgCl_2$, pH6) for 1 h, rinsed, *en bloc* stained in 2% uranyl acetate in maleate buffer (50 mM, pH 5.2) and rinsed again. Subsequently samples were dehydrated in an ethanol series and infiltrated using Epon812 resin and baked overnight at 60 °C. Sample containing resins were separated from the glass coverslip and the first few 60 nm sections from each surface were cut using a Leica UltraCut UCT. Sections were lightly stained using 2% uranyl acetate and lead citrate and viewed on FEI Tencai Biotwin transmission electron microscope at 80 Kv spot size 1. Images were taken using Morada CCD and iTEM software (Olympus).

Immunogold. Samples were fixed in 4% paraformaldehyde, 0.1% glutaraldehyde and 5 μM phalloidin at room temperature for 15 min, rinsed, and blocked in 1% fish skin gelatin and 10% normal donkey serum in PBS for 30 min. Coverslips were then incubated with the primary antibodies (rabbit anti-FBP17 1:10, or rabbit anti-dynamin 1:10) for 30 min. After rinsed in buffer for 15 min, they were incubated in secondary antibodies (12 nm or 6 nm directly conjugated gold anti-rabbit antibody) for 30 min. The samples were rinsed in PBS and then post fixed in 2.5% glutaraldehyde containing 1% tannic acid for 1 hour at room temperature, and processed as described above.

Deep-etch electron microscopy. Samples were fixed in 2% glutaraldehyde and 5 μM phalloidin at room temperature for 20 min, and processed as described previously[40].

31. Butler, M. H. *et al.* Amphiphysin II (SH3P9; BIN1), a member of the amphiphysin/Rvs family, is concentrated in the cortical cytomatrix of axon initial sSegments and nodes of Ranvier in brain and around T tubules in skeletal muscle. *J. Cell Biol.* **137,** 1355–1367 (1997).
32. Huang, B., Jones, S. A., Brandenburg, B. & Zhuang, X. Whole-cell 3D STORM reveals interactions between cellular structures with nanometer-scale resolution. *Nature Methods* **5,** 1047–1052 (2008).
33. Campbell, C., Squicciarini, J., Shia, M., Pilch, P. F. & Fine, R. E. Identification of a protein kinase as an intrinsic component of rat liver coated vesicles. *Biochemistry* **23,** 4420–4426 (1984).
34. Roux, A., Uyhazi, K., Frost, A. & De Camilli, P. GTP-dependent twisting of dynamin implicates constriction and tension in membrane fission. *Nature* **441,** 528–531 (2006).
35. Chen, H. & De Camilli, P. The association of epsin with ubiquitinated cargo along the endocytic pathway is negatively regulated by its interaction with clathrin. *Proc. Natl Acad. Sci. USA* **102,** 2766–2771 (2005).
36. Merrifield, C. J., Perrais, D. & Zenisek, D. Coupling between clathrin-coated-pit invagination, cortactin recruitment, and membrane scission observed in live cells. *Cell* **121,** 593–606 (2005).
37. Heuser, J. The production of 'cell cortices' for light and electron microscopy. *Traffic* **1,** 545–552 (2000).
38. Lin, H., Moore, M., Sanan, D. & Anderson, R. Reconstitution of clathrin-coated pit budding from plasma membranes. *J. Cell Biol.* **114,** 881–891 (1991).
39. Holroyd, P., Lang, T., Wenzel, D., De Camilli, P. & Jahn, R. Imaging direct, dynamin-dependent recapture of fusing secretory granules on plasma membrane lawns from PC12 cells. *Proc. Natl Acad. Sci. USA* **99,** 16806–16811 (2002).
40. Heuser, J. Effects of cytoplasmic acidification on clathrin lattice morphology. *J. Cell Biol.* **108,** 401–411 (1989).

CORRIGENDUM

Coupling between clathrin-dependent endocytic budding and F-BAR-dependent tubulation in a cell-free system

Min Wu, Bo Huang, Morven Graham, Andrea Raimondi, John E. Heuser, Xiaowei Zhuang and Pietro De Camilli

Nat. Cell Biol. **12,** 902–908 (2010); published online 22 August 2010; corrected after print, 26 August 2010

In the version of this letter initially published online and in print, the author affiliations were incorrect. The correct affiliations are:

Min Wu[1,2,4], Bo Huang[5,8,9], Morven Graham[2], Andrea Raimondi[1,2,4], John E. Heuser[7], Xiaowei Zhuang[5,6,8] and Pietro De Camilli[1,2,3,4,10]

[1]Howard Hughes Medical Institute, Yale University School of Medicine, New Haven, CT 06520, USA. [2]Department of Cell Biology, Yale University School of Medicine, New Haven, CT 06520, USA. [3]Department of Neurobiology, Yale University School of Medicine, New Haven, CT 06520, USA. [4]Program in Cellular Neuroscience, Neurodegeneration and Repair, Yale University School of Medicine, New Haven, CT 06520, USA. [5]Department of Chemistry and Chemical Biology, Harvard University, Cambridge MA 02138, USA. [6]Department of Physics, Harvard University, Cambridge MA 02138, USA. [7]Department of Cell Biology and Physiology, Washington University School of Medicine, 660 South Euclid Avenue, St. Louis, MO 63110, USA. [8]Howard Hughes Medical Institute, Harvard University, Cambridge MA 02138, USA.
[9]Current address: Department of Pharmaceutical Chemistry, Department of Biochemistry and Biophysics, University of California, San Francisco, CA 94158, USA.[10]Correspondence should be addressed to P.D.C. (e-mail: pietro.decamilli@yale.edu)

This error has been corrected in both the HTML and PDF versions of the letter.

nature cell biology

DOI: 10.1038/ncb2094

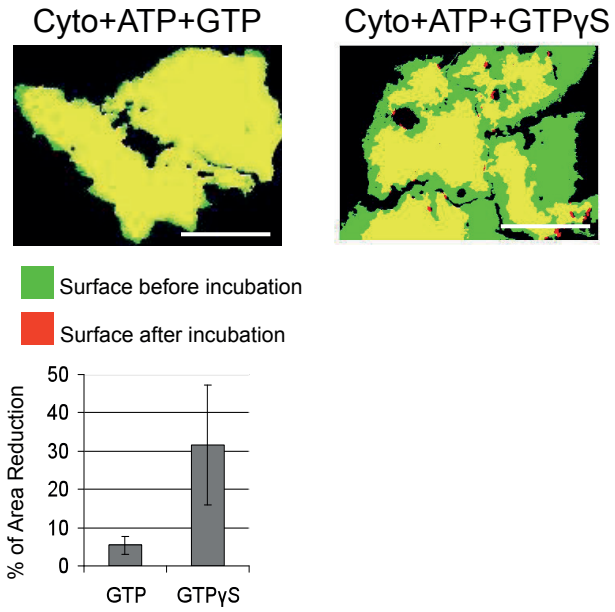

Figure S1 Reduction of the contact area between plasma membrane sheets and the substrate after incubation with cytosol, ATP plus GTP or GTPγS. Images of membrane sheets (labeled by PM-GFP) before or after incubation were converted into binary image, shown in green or red, respectively, and merged. Contact area that was lost upon incubation appears green in the merged view and area that remained appears yellow. Quantification of the reduced area was plotted in the lower panel. Data represent means ± s.d. (n = 12). Scale bars: 20 μm.

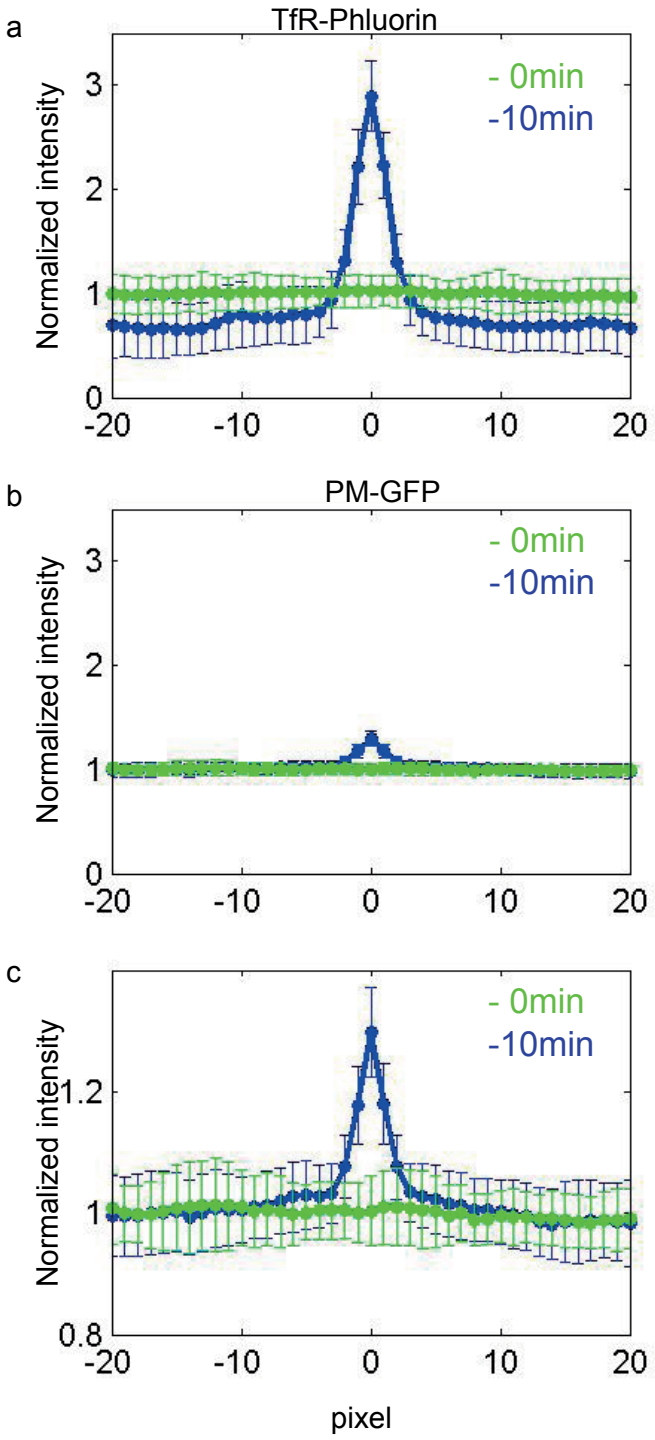

Figure S2 Clustering of transferrin receptor-pHluorin after incubation with cytosol, ATP and GTPγS is due to enrichment of the receptors. (a) Average line intensity profile of transferrin receptor-pHluorin at 10 min after incubation (blue) shows a ~3 fold increase in intensity compared to the remaining portion of the sheets. Each line profile is centered at its peak position (x=0). Data represent means ± s.d. (n = 248). The corresponding lines from the same sheets at 0 min were shown in green. Note the clustering is accompanied with a reduction of fluorescence in the remaining portion of the sheets. Both curves (0 min and 10 min) were normalized by setting the background (non-fluorescent region) as 0 and the average intensity at 0 min (green curve) as 1. (b) Average line intensity profile of PM-GFP at 10 min after incubation (blue) with the corresponding region at 0 min (green) shows a ~20% increase in intensity at clustered region and no obvious depletion in the remaining portion of the sheets. Data represent means ± s.d. (n=273). (c) The same data in (b) but plotted with a different y axis scale. (a-c) Scale: 130 nm/pixel.

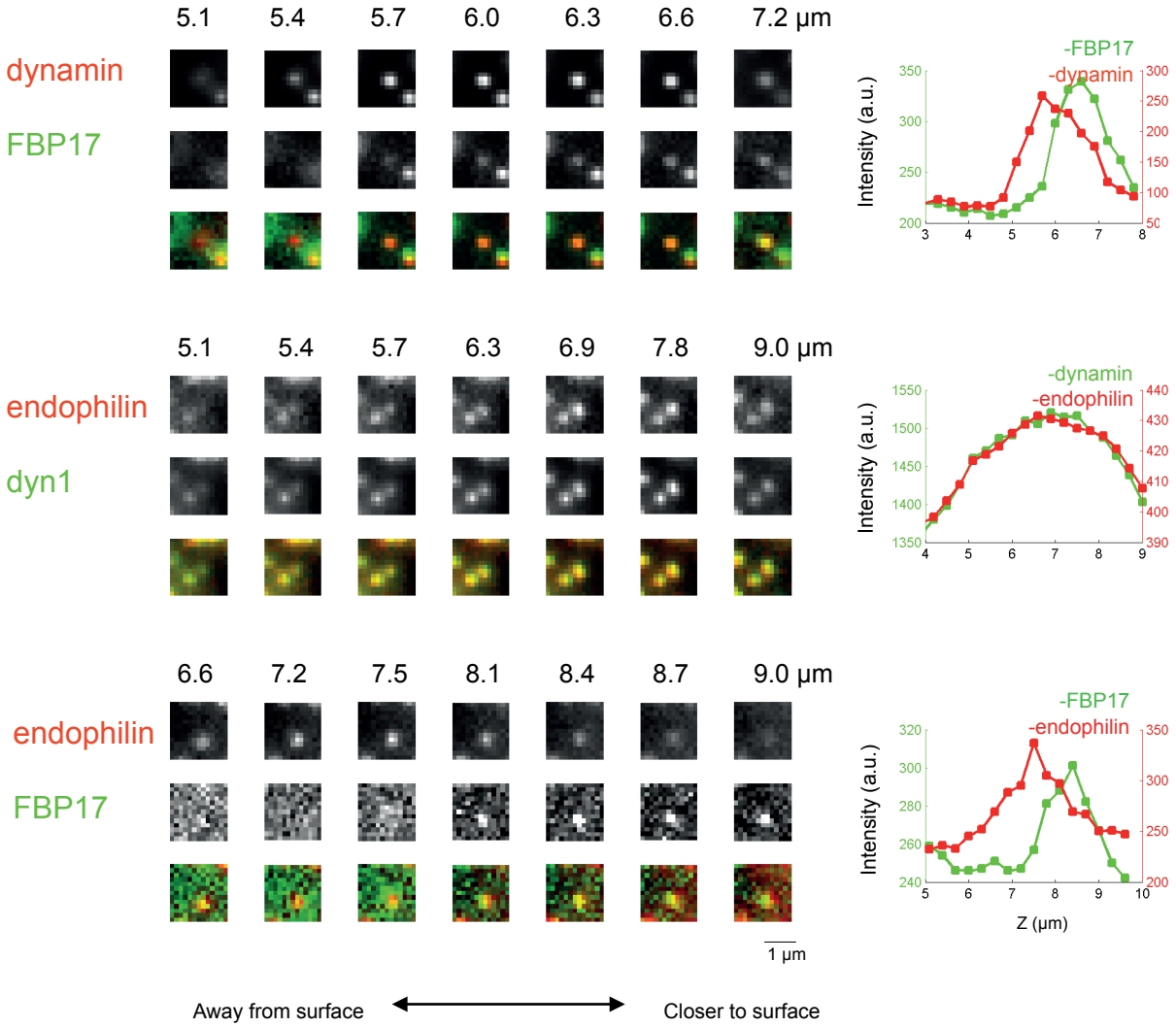

Figure S3 Comparison of the localization of endophilin, dynamin and FBP17 in membrane sheets following incubation with cytosol, ATP and GTPγS. Colocalization of endophilin (Alexa 594 endophilin) and dynamin (polyclonal antibody DG1) was observed in the *x*, *y* as well as *z* directions, in contrast to segregated FBP17 (Alexa 488 FBP17) from dynamin or endophilin in the *z* direction. Each frame of the montage is from one section of a *z* series obtained by epifluorescence imaging. The numbers above the montages indicate their relative *z* position, with the larger number corresponding to the *z* plane that is closer to the substrate (the absolute values of the *z* positions are arbitrary). Quantification of the peak intensity was shown on the right panels. Scale bars: 1 µm.

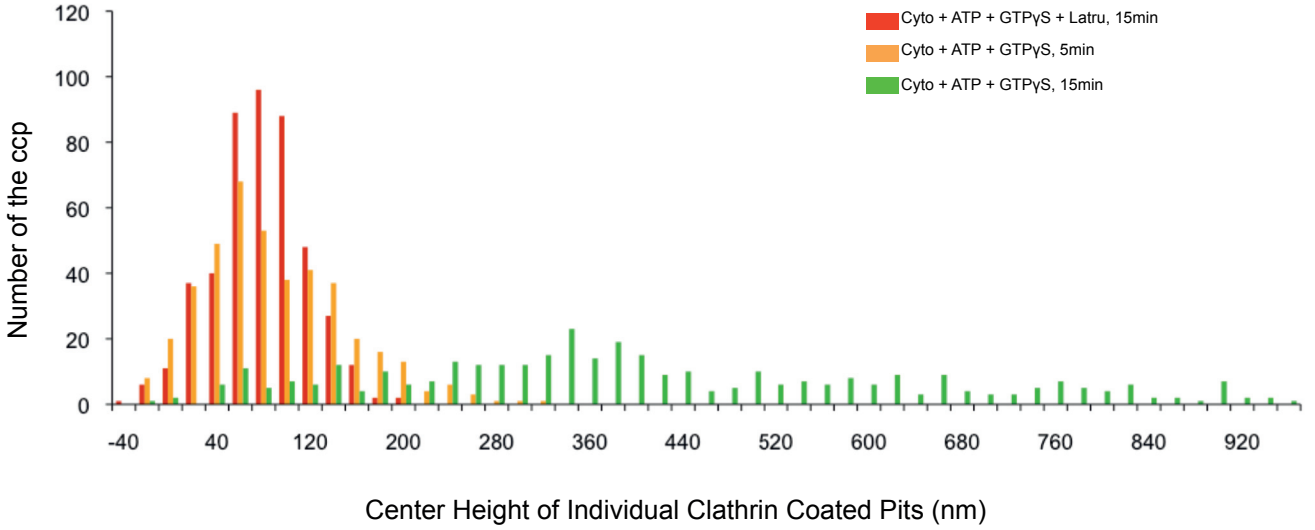

Figure S4 Distribution of the distance of clathrin-coated pits from the basal membrane under different incubation conditions. Each data point corresponded to one clathrin-coated pit. The figure shows the distance of the center position of the cluster of clathrin molecules (Alexa 405-Cy5 labeled clathrin heavy chain) that made up a given coated pit from the average position of the PM-GFP molecules (immunolabeled with Cy3-Cy5-labeled antibodies) within the sheet obtained from two-color 3D STORM images.

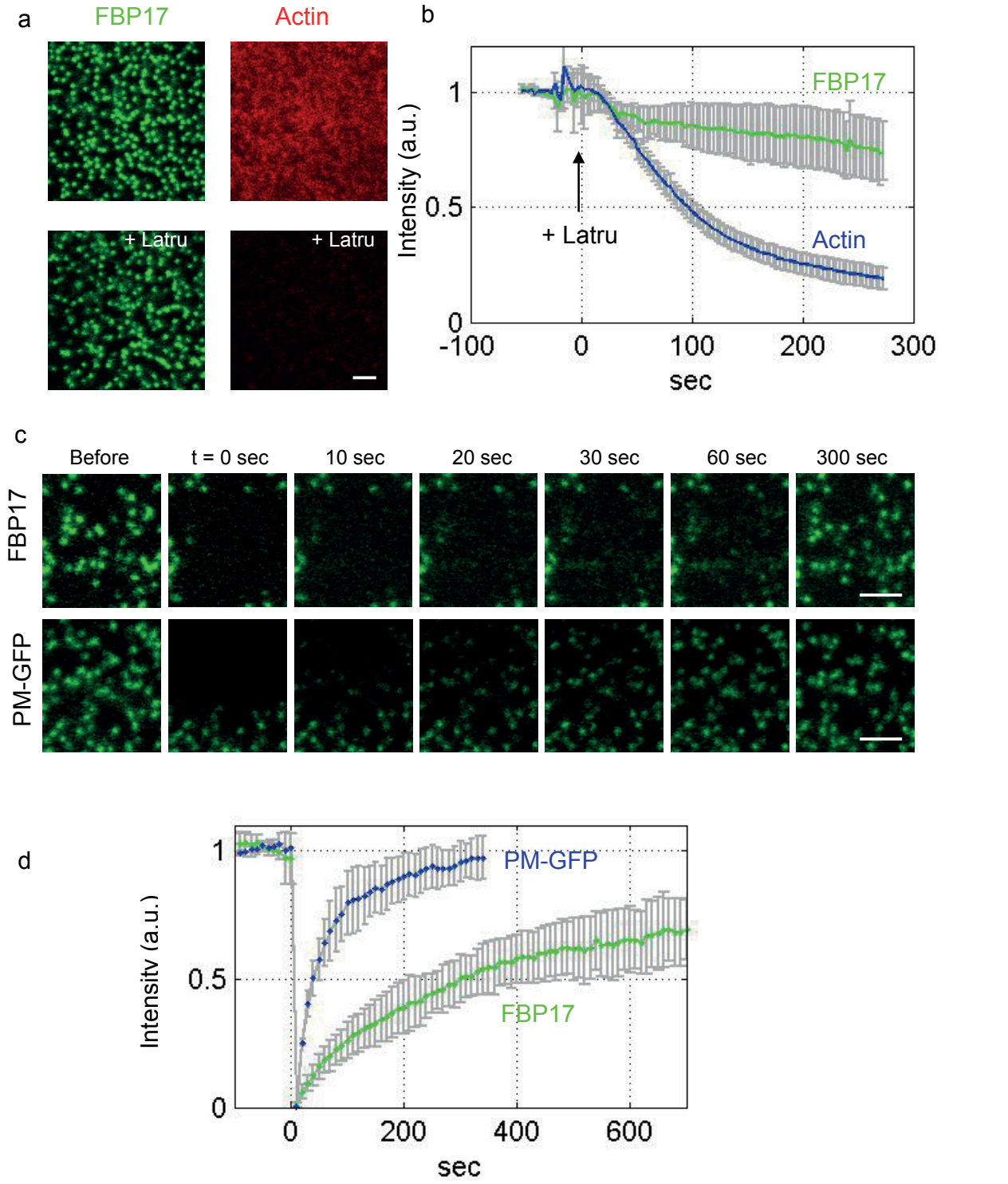

Figure S5 Stability of tubular invaginations after actin disruption. (a) Addition of latrunculin B (125 μM) to the membrane sheets after tubular invaginations have already formed led to loss of the actin cytoskeleton (labeled by Rhodamine actin) while FBP17 puncta (labeled by Alexa 488 FBP17) persisted. Fluorescent images of the same region before (t = -60 sec) and after (t = 240 sec) latrunculin B addition are shown. (b) Quantification of the integrated fluorescence intensity within an arbitrarily chosen region of interest. Data represent means ± s.d. (n=9). (c) Fluorescence recovery of PM-GFP and FBP17 puncta (Alexa 488 labeled FBP17) after photobleaching illustrated by snapshots of bleached region before and at various time points after photobleaching. (d) Quantification of the fluorescence intensity in the bleached region, after background correction and normalization. Recovery half time is 285 sec and 26 sec for FBP17 and PM-GFP, respectively. Data represent means ± s.d. (n=8). Scale bars: 2 μm.

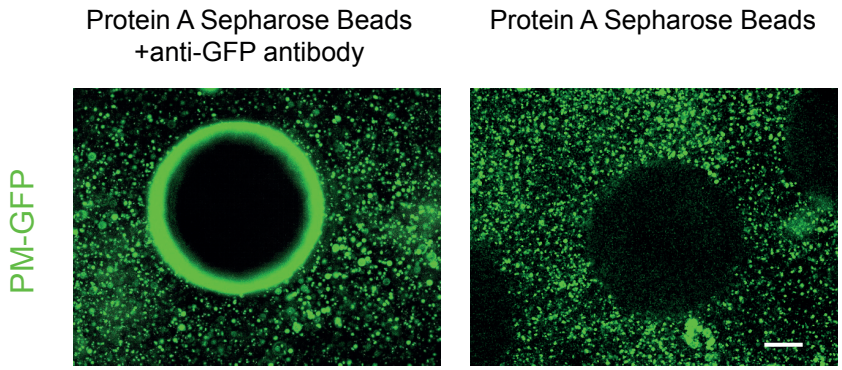

Figure S6 Capture of fissioned vesicles (PM-GFP positive) to beads coated with anti-GFP but not to uncoated beads. Each image represents the maximum intensity projection of fifty frames from a time series of epifluorescence images. Scale bars: 20 μm.

Supplementary Movie Legends

Movie S1 Membrane sheets labeled with PM-GFP upon incubation with cytosol, ATP and GTPγS exhibit dramatic transformation, with the appearance of numerous puncta and shrinking of the contact area with the substrate. The membranes were imaged at 10 sec intervals by epifluorescence microscopy and the movie is played at 20 frames per sec (200x real time).

Movie S2 Transferrin receptor pHluorin present in membrane sheets becomes significantly more clustered upon incubation with cytosol, ATP and GTPγS. The membranes were imaged at 10 sec intervals by epifluorescence microscopy and the movie is played at 7 frames per sec (70x real time).

Movie S3 3D-STORM reconstruction of membrane invaginations. Membrane sheets labeled with PM-GFP were incubated with cytosol, ATP and GTPγS for 15 min, fixed and labeled with anti-GFP, followed by secondary antibody. Scale bar: 2 μm.

Movie S4 Generation of free vesicles (PM-GFP positive) in the medium upon addition of cytosol, ATP, GTP to the intermediates generated by cytosol, ATP and GTPγS. The movie were acquired at 10 sec intervals 20 μm above the membrane by confocal microscopy and played at 20 frames per sec (200x real time).

Movie S5 Free vesicles generated in the medium upon addition of cytosol, ATP, GTP to the intermediates generated by cytosol, ATP and GTPγS are captured by beads coated with anti-GFP antibodies. Membrane sheets were from cell expressing PM-GFP and were labeled with BTR. The movie was acquired at 1 min intervals by confocal microscopy and played at 12 frames per sec (720x real time).